

Aggregation mechanisms in the adsorption of metals on Si(111)7×7E. Vasco,^{1,*} C. Polop,^{1,2} and E. Rodríguez-Cañás¹¹*Instituto de Ciencia de Materiales de Madrid, Consejo Superior de Investigaciones Científicas Cantoblanco, 28049 Madrid, Spain*²*I. Physikalisches Institut, RWTH-Aachen, D-52056 Aachen, Germany*

(Received 18 November 2002; revised manuscript received 20 March 2003; published 13 June 2003)

Several mechanisms have been revised to explain the aggregation of metal adsorbates on a 7×7 reconstructed Si(111) surface. Some of them are based on the high mobility of incident particles, while others collect the nonlocal weak or moderate interactions among adsorbates. The adsorbate aggregation, which has been characterized via the temporal evolution of the surface occupation and monomer to cluster density ratios, has been studied for each mechanism through kinetic Monte Carlo simulations as well as by approaches to the corresponding rate equations. The cooperative diffusion is revealed as the unique mechanism that is able to fit fairly the existing data related to the adsorption of metals on the Si(111)7×7 surface.

DOI: 10.1103/PhysRevB.67.235412

PACS number(s): 68.43.Jk, 68.35.Ja, 81.05.Cy

I. INTRODUCTION

In the last decade, scanning tunneling microscope (STM) studies concerning the nucleation processes on metal surfaces have reported densities of nucleated islands of orders of magnitude higher than those predicted by the mean-field theory,¹ taking into account the established diffusion parameters for these metal-on-metal systems. These quite surprising observations have taken place in homoepitaxial growths [Al on Al(111) (Ref. 2)] as well as in heteroepitaxial ones [Al on Au(111) (Ref. 3) and Ag on 2-ML-Ag/Pt(111) (Ref. 4)] where ML stands for monolayer. The discrepancy between the experimental data and the theoretical predictions has been approached by many groups, providing several explanations or models, some of which, according to the current state of the art, come from a misinterpretation of the results. For instance, some authors² have connected the phenomenon to an apparent anomalous reduction of the preexponential factor in weakly corrugated surfaces. This hypothesis that has been also supported by data achieved by other techniques,^{5,6} although not theoretically reproduced, is in forthright disagreement with that postulated by the transition-state theory^{7,8} for a thermally activated process, which predicts a preexponential factor in the THz range.^{8,9} In the Al epitaxied on Al(111) case, this disagreement has been related to the uncontrolled presence of impurities during growth.¹⁰ However, for the heteroepitaxial systems, the island density increment has been ascribed to a heterogeneous nucleation process controlled by the repulsive nature of the surface dislocations.^{3,4} Recent theoretical studies^{11,12} combining kinetic Monte Carlo (kMC) simulations and first-principles investigations have suggested the presence of nonlocal interactions between adsorbates to be responsible of this discrepancy by significantly acting upon in the surface diffusion processes and, consequently, upon the resulting morphology of the epitaxial thin films. Thus, the influence of these nonlocal interactions on the separations between adsorbates for Cu/Cu(111) has been demonstrated.^{13,14} Nevertheless, the real magnitude of the changes induced by these nonlocal interactions in the nucleated island density is still to be elucidated.¹⁵ The current controversy created around this topic inspires an increasing number of studies about the in-

fluence of the nonlocal interactions between adatoms and/or clusters on the nucleation and growth processes on metal surfaces.

The nature and range of the interactions among adsorbates as well as the possible substrate mediations, which provide indirect interaction mechanisms, are issues that have been extensively studied for homoepitaxial metal systems. Beyond the chemical bonds between adsorbates, the presence of two types of electrostatic long-range interactions for adsorbate pairs has been established: (i) attractive interactions driven by the van der Waals forces and (ii) repulsive interactions between multipoles that arise in each adsorbate due to surface-induced charge redistribution in each one of them. On the other hand, two kinds of substrate mediations have been considered for these systems: (a) An oscillatory indirect electronic interaction originated by the scattering of the two-dimensional nearly free electron gas on the substrate surface for the adsorbates, which generates standing-wave patterns in the electron density that gives rise to interactions between scatterers; and (b) a repulsive elastic interaction that arises from adsorbate and substrate relaxations mediated via the atomic lattice.

On the contrary, there is very little information about the nonlocal interactions between adsorbates on semiconductor surfaces and, in particular, concerning the nature of substrate-mediated interactions. In contrast with metals, semiconductor materials usually present a highly corrugate potential energy surface for adsorbates due to the presence of localized electronic states. In particular, the Si(111)7×7 surface characterized by high-energy hopping barriers (~0.7–1.0 eV) (Ref. 16) at the borders of the large triangular half cells constitutes an example of it. In spite of the fact that the high hopping barriers should sensibly reduce the diffusion rate, an unexpected tendency (unexplainable under a hit-and-stick model)^{17,18} of the adsorbates to aggregate inside the half cells at room temperature (RT) at relatively short times has been previously described and established.^{17–20} Then, this surprising behavior for adsorbates on reconstructed semiconductor surfaces suggests the presence of attractive nonlocal interactions between adsorbates promoting the cluster formation via the reduction of the hopping barriers.

Several direct experimental evidences for the adsorption

of Pb,¹⁹ Sn,²⁰ and Y (Ref. 18) atoms on the Si(111)7×7 surface reinforce the nonlocal interaction suggestion. In the three inspected systems, the single adatoms (monomers), which constitute the unique mobile species at RT, diffuse preferably toward the occupied nearest-neighboring half cells. In the case of the Pb atoms,¹⁹ it has been demonstrated by real time STM movies how monomers jump faster toward a neighboring half cell occupied by other adatoms than toward empty half cells. The difference between hopping rates is maximized for the Sn atom adsorption,²⁰ in which monomers jump at RT only to the occupied neighboring half cells, and no jumps to free halves were detected in spite of long periods of observation (2–3 h). In the Y atom adsorption case,¹⁸ STM images show that most of the half cells occupied by monomers are surrounded by empty triangular cells pointing out to the fact that whenever an atom lands in a free half cell with at least an occupied neighboring half cell, it tends to diffuse toward this neighboring half cell, and thus only those adatoms surrounded by empty half cells remain as individual atoms during the whole measurement time. From these three independent observations, it is derived that the diffusive behavior of monomers and, therefore, their strong tendency to agglomerate are influenced (but governed) for some kind of effective interaction of attractive nature among adsorbates localized in the nearest-neighboring halves.

In the frame of the preceding controversy, the aim of this work is to study the atomic mechanisms that can promote the fast aggregation, controlled or not by nonlocal interactions, of the metal adsorbates inside the half cells of the 7×7 reconstructed Si(111) surface at RT. The aggregation capacity of the adsorbates for each mechanism will be examined through kMC simulations as well as by approaches to the corresponding rate equations. The independent model used for the kinetic Monte Carlo simulations is presented in Sec. II. In Sec. III, the aggregation rate equations are introduced and progressively modified in order to include the effects of each mechanism. The behavior of the proposed equations is investigated through the numeric solutions feasible of being computed and is estimated for all mechanisms by means of the kMC-simulated curves. Further, the existent experimental data concerning the adsorption of Pb,¹⁹ Ag,^{17,21,22} and Y (Ref. 18) atoms on the Si(111)7×7 surface are reproduced by kMC simulations in a way alternate to the proposal by the corresponding authors. Finally, the fair fitting of the experimental data by using a unique aggregation mechanism is discussed, suggesting for the existence of a common model that is generalizable for similar systems.

II. MODELING THE POTENTIAL ENERGY OF THE 7×7 RECONSTRUCTED SI(111) SURFACE

The Si(111)7×7 surface is formed by a honeycomb lattice of large triangular unit half cells with alternate stacking faults (fault f and unfault u cells) separated by dimer rows and advacancies. It is experimentally observed that the metal-adatom adsorption at RT occurs preferably inside the half cells without being strongly trapped, in many cases,²³ into the inner adsorption sites of the half cell; i.e., the monomers move quasifreely inside the half cell, only confined by

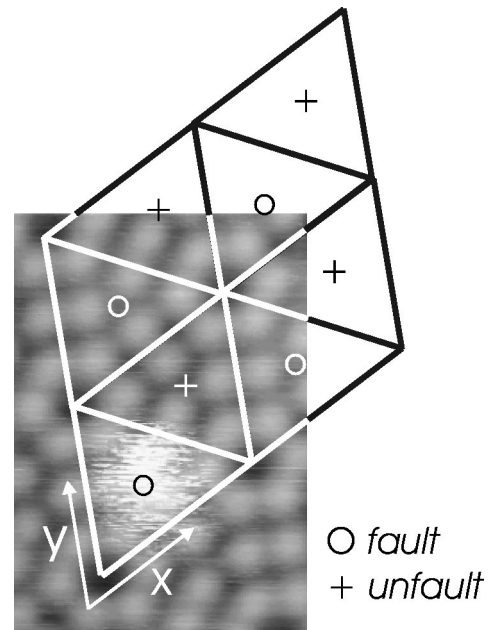


FIG. 1. Fuzzy appearance of an oscillating Y monomer trapped inside a faulted half cell (taken from Ref. 18). The point lattice employed to model the Si(111)7×7 surface is superimposed to the image.

the dimer rows. This kinetic behavior confers to the monomer a rather fuzzy or noisy aspect (see Fig. 1), which has been ascribed to the oscillation of the adatom among the different adsorption sites at much faster rates than the STM scanning frequency.^{18,19} The fuzzy appearance of a monomer reveals that the intracell hopping energy barriers among adsorption sites are lower than the intercell ones, and thus, the surface diffusion will be governed by these latter barriers. Consequently, the potential-energy diagram of this surface can be simplified neglecting the intracell diffusion barriers as shown in Fig. 2(a). Then, the aggregation of several adatoms inside one half cell can be considered as a “nucleation” process. Thus, our simulation scheme, which is schematically represented (superimposed) in Fig. 1, uses the unit half cell as the basic unit of the surface lattice and ignores all processes operating at smaller length scales.

In the model, the atoms are deposited with a rate of F ; diffused at a rate of D ; and agglomerated in the half cells of the Si(111)7×7 surface at a rate of $\partial O/\partial t$, where the occupation O represents the ratio of the number of half cells occupied during the growth experiment to the total number of half cells on the surface, so that $0 \leq O \leq 1$. To every lattice site that is used to model the reconstructed surface, two parameters are assigned: an indicator of the presence of stacking fault (f or u) and the number of atoms n adsorbed inside it which forms the “nucleated cluster”. The nucleation is simulated by considering the diffusion process between half cells, while the detailed description of an adatom movement inside the half cell is omitted. Only hops of monomer through the dimer rows of the 7×7 reconstruction between adjacent half cells are allowed. These thermally activated hops take place at a frequency given by $\nu = \nu_0 \exp(-\chi_{ij}/k_B T)$; χ_{ij} being, the diffusion activation energy to jump

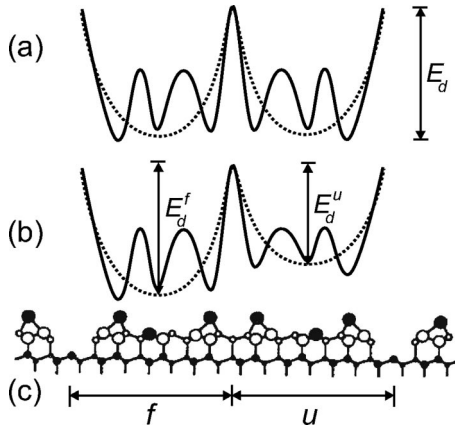


FIG. 2. (a) Schematic representation of the potential-energy diagram of a unit cell (solid line) and its approximation to a diagram simplified to two adsorption sites (dotted line). (b) Diagram (solid line) and two-site approximation (dotted line) of the potential energy of a unit cell taking into account the energy asymmetry to escape from faulted and unfaulted half cells. (c) Cross section of the Si(111)7 \times 7 unit cell in the dimer-adsorbate staking fault (DAS) model.

from site i to j ; k_B the Boltzmann's constant; T the substrate temperature; and ν_0 the preexponential factor. ν_0 is assumed to be the same for faulted and unfaulted unit half cells.

If in the first approach, any nonlocal interaction between adatoms and/or clusters is neglected, χ_{ij} will depend on the energy barrier E_d to jump among half cells as well as the energy barrier to detach the adatom from the source cluster E_i ; such that $\chi_{ij} = E_d + E_i$. This first case corresponds to the random-walk diffusion in which the probability of an adatom to diffuse to any of the three neighboring half cells of the source half cell is the same, independent of the occupation state of them. E_i is coupled to intracell adatom-adatom interaction E_{huc} as a linear function of the number of bonds among the adatoms that form one cluster. The model assumes that all the adatoms inside a half cell interact with each other to form a maximum number of bonds (n_{sat}) so that in an n -size cluster (with $n \leq n_{sat}$) each atom has $n-1$ bonds. If E_b represents the "effective" binding energy per bond, the detachment energy of an adatom from an n -size cluster is given by $E_i = -E_{huc} = (n-1)E_b$ for $n \leq n_{sat}$ and $E_i = n_{sat}E_b$, otherwise. Whereas each half cell has a maximum capacity for adsorbed adatoms, as pointed out by the experimental results,^{17,18} a repulsive regime with $E_i = -E_{huc} \rightarrow -\infty$ is included in the intracell interaction energy curve in order to simulate the instability of the clusters with sizes larger than n_{max} . Figure 3 shows a representative outline of the dependence of intracell interaction energy on the number of inner adatoms.

To simulate the nonlocal attractive interaction between adatoms adsorbed on different half cells, the occupation states of the initial and final positions before $\{E_i = -E_{huc}(n_i)\}$ and after $\{E_j = E_{huc}(n_j+1)\}$ the jump must be considered. Thus, the presence of adatoms in the nearest-neighbor half cells leads to the reduction of the diffusion activation energy, which favors the aggregation of the adatoms. In the cooperative diffusion, as we name this diffu-

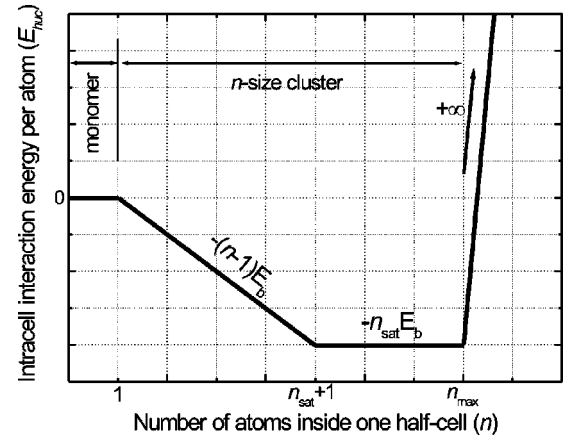


FIG. 3. Dependence of the potential energy of a half cell on the number of adatoms trapped on it.

sion hereafter, the surface migration is modeled as a hopping process with an activation energy given by $\chi_{ij} = E_d + (E_i + kE_j) = E_d + (n_i - 1 - kn_j)E_b$, ($n_i - 1$) and n_j being the number of effective bonds in the source and target half cells before and after the jump, respectively. k represents a spatial attenuation factor of the substrate-mediated non-local interactions, which contains information about the interatomic attraction potential between adsorbates on the 7 \times 7 reconstructed Si(111) surface. In the extreme case where $k \rightarrow 0$, the behavior of the cooperative diffusion tends to the random-walk diffusion. Note that the cooperative diffusion is, in principle, anisotropic, since the jump direction is determined by the occupation states of the possible destination half cells.

A tendency to the agglomeration with a preference for faulted half cells has been previously observed in several systems.^{17,18} These results suggest a difference between the hopping energy barriers to escape from the fault and unfault half cells. In order to include this experimental evidence in our model, different surface contributions for the fault (E_d^f) and unfault (E_d^u) half cells have been contemplated, being, in general, $E_d^f \neq E_d^u$. Then, the potential surface diagram shown in Fig. 2(a) has been modified [Fig. 2(b)] to incorporate the asymmetry between the fault and unfault half cells.

The kMC simulations were performed on a 150 \times 150 half-cell lattice with periodic boundary conditions. To simplify our diffusion model, a spatial attenuation factor $k=1$ has been chosen. The parameters used to shed light on the model (i.e., $F=0.01$ ML/s, $E_d^f=E_d^u=0.8$ eV, $E_b=0.1$ eV, $\nu_0=5 \times 10^9$ s $^{-1}$, and $T=300$ K) are included, as it will be shown further in Sec. IV, in the range of characteristic values of the diffusion and aggregation of metal adsorbates on the Si(111)7 \times 7 surface. The simulation of the diffusion processes includes the relaxation during 4 h of the previously grown surface in order to take into account the experimental delay between the phases of thermal evaporation and STM measurements. In the model, only the single-atom movement is allowed, while the displacement of the whole cluster is inhibited, and the aggregation becomes irreversible only for clusters with sizes larger than the critical size i^* . The simulated data were averaged over more than 20 runs.

III. RANDOM INCIDENCE

In the following, we are going to develop the rate equations that describe the evolution of the surface occupation driven by different aggregation/desaggregation mechanisms. The random incidence, in which the incident atom remains in the landing half cell without relaxing, is the simplest of them. The temporal evolution of the surface occupation driven by the random incidence presents the following form:

$$\begin{aligned} \frac{\partial O}{\partial t} &= \gamma F(1-O) \Rightarrow O(t) = 1 - \exp(-t/\langle t \rangle) \\ &\equiv O(\theta) = 1 - \exp(-\gamma\theta), \end{aligned} \quad (1)$$

such that for $t \gg \langle t \rangle$, $O \rightarrow 1$; $\langle t \rangle = 1/\gamma F$ being the average time among the successive arrival of two atoms to the same half cell; F the deposition rate (ML/sec); $\gamma = 24.5$ the number of atoms of a 1×1 structure per half cell of the Si(111)7 \times 7 surface; and $\theta = Ft$ the fractional coverage referred to the 1×1 layer. Thus, the incident particle has a probability of $(1-O)$ to impinge on a free half cell, and the landing process occurs γF times per second on a half cell.

Since the experimental evidences demonstrate that the half cells have the maximum capacity to accommodate adsorbates,^{17,18} Eq. (1) must be modified as follows. If ρ_{\max} represents the maximum-size cluster density and $\langle t \rangle_{\max} = n_{\max}/\gamma F = n_{\max}\langle t \rangle$, the average time of formation of such clusters from random incidence; then the probability of one incident particle to land on a half cell occupied by a maximum-size cluster (saturated half cell) becomes ρ_{\max} . This particle will bounce back from the saturated half cell either toward those $(1-O)$ empty half cells, or toward those $(O-\rho_{\max})$ half cells occupied by clusters with sizes lower than n_{\max} (submaximum-size cluster), or toward those $\approx \rho_{\max}$ remaining half cells that are saturated by the maximum-size clusters. These bounce-back processes occur with probabilities $(1-O)\rho_{\max}$, $(O-\rho_{\max})\rho_{\max}$, and ρ_{\max}^2 , respectively, around an average coverage $\langle \theta \rangle_{\max} = F\langle t \rangle_{\max} = n_{\max}/\gamma$. As a result of the bounce-back to a saturated half cell, a second bounce-back process takes place toward an empty half cell [with a probability $(1-O)\rho_{\max}^2$], a submaximum-size cluster [$(O-\rho_{\max})\rho_{\max}^2$], or a maximum-size cluster (ρ_{\max}^3). Thus, by developing the probability series for infinite bounce-back processes and adding all the favorable contributions to the increment of the occupation, Eq. (1) becomes

$$\frac{\partial O}{\partial t} = \gamma F(1-O) \sum_{p=0}^{\infty} \rho_{\max}^p = \gamma F \left(\frac{1-O}{1-\rho_{\max}} \right). \quad (2)$$

In the same way, the rate equation that describes the monomer density, ρ_1 , evolution driven by random incidence, taking into account the maximum capacity of the adsorbates per half cell is given as

$$\frac{\partial \rho_1}{\partial t} = \gamma F \left(\frac{1-O-\rho_1}{1-\rho_{\max}} \right), \quad (3)$$

where the term $-\rho_1$ included in the upper parentheses is linked to the direct landing on the half cells occupied by

monomers. Note that the bounce-back process has been included in Eqs. (2) and (3) as a part of the random incidence, which means that this has been assumed as an instantaneous process without interfering in the deposition rate.

In order to solve numerically Eqs. (2) and (3), the temporal dependence of the maximum-size cluster density should be known. By including the incidence redistribution through bounce backs, $\rho_{\max}(t)$ can be approached to $\rho_{\max}(t) \propto 1 - (1 - \gamma F n_{\max}^{-1} t)^{1/2}$, which is the solution of the rate equation $\partial \rho_{\max} / \partial t = \gamma F [2n_{\max}(1 - \rho_{\max})]^{-1}$. The nontendency to the saturation of the function $\rho_{\max}(t)$ is due to considering the arrangement of the impinging atoms on the surface through a physically unlikely infinite series of successive bounce backs. If the number of successive bounce backs is limited to a physical-meaning value p (for instance $p=2$, as it has been implemented in our simulation code), a saturation tendency appears as a result of the appearance of compact groups of ten or more maximum-size clusters. These groups block the bounce backs from their central positions, making feasible the formation of clusters (overclusters) with size larger than n_{\max} . The formation probability of such overclusters is then $\propto \rho_{\max}^{3p}$. In the frame of these approaches, ρ_{\max} evolves according to $\partial \rho_{\max} / \partial t = \gamma F(1 - \rho_{\max}^{3p}) [2n_{\max}(1 - \rho_{\max} + \rho_{\max}^{3p})]^{-1}$.

The bounce-back process constitutes a desaggregation mechanism that tends to spread out the particles on the Si(111)7 \times 7 surface, increasing its occupation for a given coverage. Nevertheless, the particle redistribution capacity of these processes is slightly even for an n_{\max} as low as three atoms per half cell, ($\langle \theta \rangle_{\max} \approx 0.12$). The moderate effect of the bounce backs on the occupation evolution (represented vs coverage) for different maximum capacities is shown in Fig. 4(a). The bounce-back processes produce an influence more significantly on the monomer to cluster densities ratio $\rho_1 / (O - \rho_1)$, as revealed in Fig. 5(a). As n_{\max} decreases, the $\rho_1 / (O - \rho_1)$ ratio also decreases as a result of the particle redistribution from the random incidence. Bowing deviations [i.e., changes in the $\rho_1 / (O - \rho_1)$ decreasing slope] appear after the first bounce backs. This behavior suggests that a significant fraction of the bounced-back particles become monomers once they are adsorbed on its final state, counterbalancing partially to the aggregation process.

IV. AGGREGATION MECHANISMS

A. Capture area versus transient mobility

Each cluster is surrounded by an area for the capture of incident particles, or the impinging particle is able to travel an average distance of R half cells (thermalization path) before accommodating on the substrate surface, transferring progressively its excess of kinetic energy to the substrate.

The major difference between these two mechanisms lies while the capture area assures the aggregation to a center that corresponds to the global energy minimum of the attaching area, in the transient mobility, the local and global energy minima compete between them for the landing particle as a function of their proximities to the land site. Thus, the near-

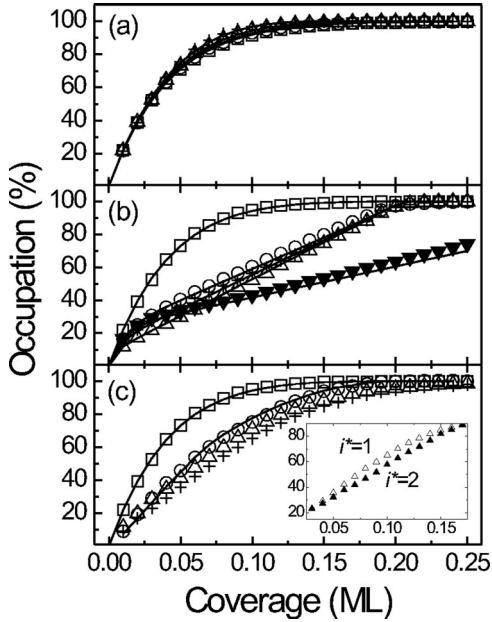


FIG. 4. Dependence of the surface occupation on the coverage for different mechanisms. The symbols correspond to the kMC-simulated data and the lines represent the numerical solution of the corresponding rate equations. (a) Behavior of the random diffusion for different maximum capacities of adsorbates per half cell (n_{max} : \square , 20; \circ , 10; \triangle , 5; and $+$, 3). (b) Behavior of the transient mobility for several thermalization radii (open symbols correspond to different combination of R and r with $n_{max}=5$: \square , $R=r=0$ (random incidence); \circ , $R=r=1$; $+$, $R=2$ and $r=1$; and \triangle , $R=r=2$; while \blacktriangledown identifies to the data for $R=r=1$ and $n_{max}=10$). (c) Behavior for different diffusion types assuming $n_{max}=5$: \square , random incidence; \circ , random diffusion; \triangle , oriented diffusion; and $+$, cooperative diffusion. Inset in (c): Dependence of surface occupation on the critical size (i^*) for the cooperative diffusion.

est local minima are more favorable than the most distant global ones. Taking into account that the aggregation to these local minima can be irreversible, this difference justifies an aggregation capacity for transient mobility lower than that of the capture area. Nevertheless, the capture of the impinging particles by the clusters is better understood in the frame of the diffusion mechanisms, since this is probably linked to noninstantaneous mobility oriented by attractive interactions. Then, we prefer to approach the capture area mechanism further in the section devoted to diffusions.

In the transient mobility, the path and thermalization time of the impinging particles depend on their kinetic energies as well as the energy dissipation rate, which is mainly mediated by coupling to the substrate phonons.²⁴ This mechanism is favored by using nonthermodynamic equilibrium deposition techniques, such as sputtering, pulsed laser deposition, and ionic implantation in which very energetic particles are generated.²⁵ On the other hand, the directional nature of characteristic bonds of the semiconductor reconstructed surfaces can delay the energy transference between the impinging particles and the substrate connecting with the incidence angle. So, this aggregation mechanism enhanced by the slow

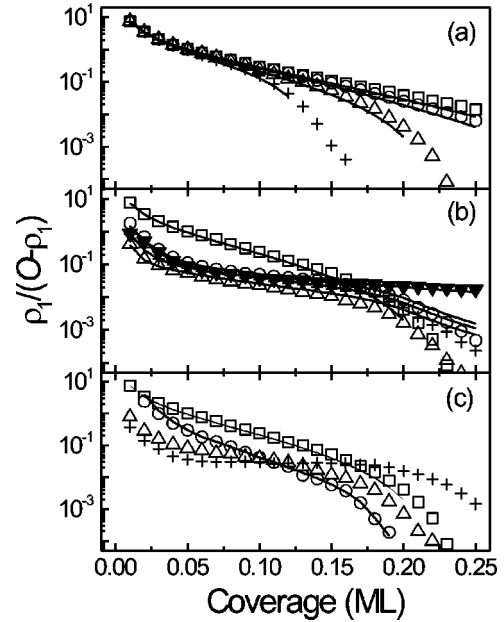


FIG. 5. Dependence of the monomer to cluster densities ratio on the coverage for different mechanisms. The symbols correspond to the kMC-simulated data and the lines represent the numerical solution of the corresponding rate equations. (a) Behavior of the random diffusion for different maximum capacities of adsorbates per half cell (n_{max} : \square , 20; \circ , 10; \triangle , 5; and $+$, 3). (b) Behavior of the transient mobility for several thermalization radii (open symbols correspond to different combination of R and r with $n_{max}=5$: \square , $R=r=0$ (random incidence); \circ , $R=r=1$; $+$, $R=2$ and $r=1$; and \triangle , $R=r=2$; while \blacktriangledown identifies to the data for $R=r=1$ and $n_{max}=10$). (c) Behavior for different diffusion types assuming $n_{max}=5$: \square , random incidence; \circ , random diffusion; \triangle , oriented diffusion; and $+$, cooperative diffusion.

thermalization of incident energetic particles can be significantly faster than the typical diffusive mechanisms operating in quasiequilibrium regimes.

A thermalization path of R half cells means that the impinging particle can, in principle, attach to any cluster nucleated in the area $A(R)$ around the land site. However, this does not imply that the clusters nucleated inside and/or outside the $A(R)$ produce an influence, in the same way, on the instantaneous jump direction of the mobile particles. Then, if an energetic impinging particle is able to jump up to the R neighboring half cells but during each hop its jump direction is biased by the r neighboring half cells, an effective $A(R)$ for the Si(111) 7×7 surface can be defined as $A(R,r) = \sum_{q=1}^R 3q(1/3)^{f(q-r)} + 1$, where $f(x) = x$ for $x \geq 0$ and $f(x) = 0$ otherwise; such that if $R \leq r$, $A(R) = 3R(R+1)/2 + 1$. Then, Eq. (1) takes the form

$$\frac{\partial O}{\partial t} = \gamma F(1 - A(R)O) \Rightarrow O(t) = \frac{1}{A(R)} [1 - \exp(-t/\langle t \rangle_t)], \quad (4)$$

such that for $t \gg \langle t \rangle_t$, $O \rightarrow 1/A(R)$. As a result of this mechanism, the nucleation area is not more than the half cell but it becomes $A(R)$ half cells with a shorter nucleation average

time $\langle t \rangle_i = 1/A(R) \gamma F$. By introducing the maximum capacity per half cell, Eq. (4) is modified to

$$\frac{\partial O}{\partial t} = \gamma F \frac{\{1 - A(R)O - \rho_{\max}[1 - A(R)]\}}{(1 - \rho_{\max})}, \quad (5)$$

and ρ_1 evolves according to

$$\frac{\partial \rho_1}{\partial t} = \gamma F \frac{\{1 - A(R)(O + \rho_1) - \rho_{\max}[1 - A(R)]\}}{(1 - \rho_{\max})}. \quad (6)$$

Note that there is not a nucleation area around the maximum-size clusters, and that the tendency to the maximum occupation $O \rightarrow 1$ is a consequence of the bounce-back processes. By considering the incidence as to a deterministic process, the number of maximum-size clusters would rise as a step function of the deposition time according to $\rho_{\max}(t) = q/A(R)$ for any t ranged in $qn_{\max}(t)_i < t < (q+1)n_{\max}(t)_i$, with q taking integer values $q=0,1,2,\dots,A(R)-1$. In this case, an approach to a linear $\rho_{\max}(t)$ dependence as $\rho_{\max}(t) = t/\langle t \rangle_{\max}$ is appropriate.

The transient mobility represents an efficient aggregation mechanism whose magnitude is modulated by the incorporation ratio, as shown in Fig. 4(b). Two different increased regimes are observed in the evolution of the occupation with the coverage: for very low coverages, an exponential rise behavior, which is governed by the incidence and formation of new nucleation centers on the free-substrate surface, followed by a linear increased regime controlled by the aggregation to the previously established clusters and creation of the new ones from the bounce-back phenomenon. Therefore, in the second regime the occupation follows a coverage dependence similar to the $\rho_{\max}(\theta)$ dependence. The transient mobility powers the quick appearance of the bounce-back processes by reducing the coverage in which the bounce-back process appears in an $A(R)$ factor [i.e., $\langle \theta \rangle_{\max} = n_{\max}/\gamma A(R)$]. All occupation curves with the same n_{\max} reach the saturation value for a similar coverage $\theta_{sat} \approx n_{\max}/\gamma$ due to the lack of nucleation area around the maximum-size clusters.

Figure 5(b) shows that $\rho_1/(O - \rho_1)$ ratio decreases for a given coverage as $A(R)$ increases (for $R > 0$) due to the enhancement of the aggregation process. Three regimes with different decreasing slopes are isolated: The first regime is characterized by an abrupt reduction of monomer density that can be ascribed to the formation of initial clusters, which become the first aggregation centers. Subsequently, the ρ_1 decrease rate is reduced as a result of the appearance of new monomers from the bounce-back phenomenon. Once all the half cells are occupied ($O = 1$), the bounce back ceases producing new monomers, originating again an increase in the ρ_1 decrease rate.

B. Random diffusion

In this mechanism, the probability of the diffusing particle to jump toward any of its three nearest-neighbor half cells is the same (i.e., $1/3$) with the independence of their occupation states. It originates a net isotropic diffusion process on the Si(111) 7×7 surface. Thus, the nucleation process in this

regime is only achieved as a function of the ability of the adatoms confined inside the same half cell to be bound among them. For $i^* = 1$, O and ρ_1 evolve according to

$$\frac{\partial O}{\partial t} = \gamma F \frac{(1 - O)}{(1 - \rho_{\max})} - D\sigma\rho_1 \sum_{n=1}^{n_{\max}-1} \rho_n \equiv \gamma F \frac{(1 - O)}{(1 - \rho_{\max})} - D\sigma\rho_1(O - \rho_{\max}) \quad (7)$$

and

$$\frac{\partial \rho_1}{\partial t} = \gamma F \frac{(1 - O - \rho_1)}{(1 - \rho_{\max})} - D\sigma\rho_1(O + \rho_1 - \rho_{\max}), \quad (8)$$

where $D = D_0 \exp(-\chi/k_B T)$ being the monomer diffusion coefficient for the hop between adjacent half cells; $\chi = f(E_d, E_i)$ the process activation energy that reduces to $\chi = f(E_d)$ for $i^* = 1$; and σ , the capture number that describes the probability per time and diffusivity unit of monomer capture by other monomers or existing clusters. In principle, for the point-island model proposed in this work, the capture probability does not depend explicitly on the cluster size and thus σ can be moved outside the sum over cluster sizes in Eq. (7).

C. Cooperative diffusion

In this second diffusion type, the probability of the diffusing particle to hop toward a neighboring cell becomes dependent on the occupation state of the target position. Thus, the isotropic nature of the diffusion process vanishes, originating diffusive surface currents toward the nucleation centers. In this case, the aggregation rate for $i^* = 1$ can be rewritten as

$$\frac{\partial O}{\partial t} = \gamma F \frac{(1 - O)}{(1 - \rho_{\max})} - \sigma\rho_1 \sum_{n=1}^{n_{\max}-1} D_n P_n^* \rho_n. \quad (9)$$

The subindex n is associated to the diffusion of a monomer to an n -size cluster, then $D_n = D_0 \exp(-\chi_n/k_B T)$ being the diffusion coefficient of this process; and P_n^* , its normalized directional capture probability that is differentiated by the size of the target cluster in the following form:

$$P_n^* \propto \frac{\exp(-\chi_n/k_B T)}{\sum_{m=1}^{n_{\max}-1} \exp(-\chi_m/k_B T)} = \left[\sum_{m=1}^{n_{\max}-1} \exp(\Delta\chi_{nm}/k_B T) \right]^{-1}, \quad (10)$$

where $\Delta\chi_{nm} = \chi_n - \chi_m$. Consequently, an effective ‘‘size-dependent’’ capture number for the point islands can be defined as $\sigma_n = \sigma P_n^*$. In general, the activation energy ascribed to a cooperative diffusion is given as $\chi_n = f(E_d, E_i, E_j)$, simplified to $\chi_n = f(E_d, E_j)$ for $i^* = 1$. Afterwards, according to our model: $\chi = E_d + (E_i + kE_j)$. As a consequence of the cooperative diffusion, the monomer density decreases, biased by the aggregation centers according to

$$\frac{\partial \rho_1}{\partial t} = \gamma F \frac{(1 - O - \rho_1)}{(1 - \rho_{\max})} - 2D_1\sigma_1\rho_1^2 - \sigma\rho_1 \sum_{n=2}^{n_{\max}-1} D_n P_n^* \rho_n. \quad (11)$$

D. Oriented diffusion

Note that when an additive approach to the jump activation energy of the form $\chi_n = E_d + (\alpha E_i + \beta E_j)$ is assumed, the dependence between the jump probability and the corresponding activation energy $P_n^* \propto \exp(-\chi_n/k_B T)$ can be reduced to $P_n^* \propto \exp(-\beta E_j/k_B T)$. This is a consequence of the fact that for the same source cell, $\Delta\chi_{ij}$ ($i = \text{const}$, $j = 1, \dots, 3$) becomes only a function of E_j . The additive form of the activation energy matches our simulation (with $\alpha = 1$ and $\beta = k$) as well as the assumption proposed by Fichthorn and Scheffler¹¹ based on considering a linear potential of repulsion between adjacent adsorption sites ($\alpha = \beta = 1/2$). On the other hand, if the system satisfies the condition $\beta E_j \ll E_d + \alpha E_i$, which can be fulfilled for weak nonlocal interactions, the jump activation energy reduces to $\chi_n \approx E_d + \alpha E_i = \chi_{\text{random diffusion}}$. This implies that the diffusion coefficient does not depend on E_j (i.e., $D_n = D$). Then, the created decoupling among the energetic dependences of the jump probability and the diffusion coefficient for a given hop direction would originate a paradoxical situation unable of being reproduced through the standard kMC simulation algorithms. Thus, this diffusion type in which the particles move, biased by the aggregation centers hopping between adjacent half cells at the jump frequency corresponding to the random diffusion, is hereafter termed as oriented diffusion. The rate equation that describes this case can be deduced by considering a unique diffusion coefficient in Eq. (10), such that for $i^* = 1$,

$$\frac{\partial O}{\partial t} = \gamma F \frac{(1-O)}{(1-\rho_{\max})} - D \sigma \rho_1 \sum_{n=1}^{n_{\max}-1} P_n^* \rho_n. \quad (12)$$

In the same way, the monomer density evolution can be modified to gather this diffusion type:

$$\frac{\partial \rho_1}{\partial t} = \gamma F \frac{(1-O-\rho_1)}{(1-\rho_{\max})} - 2D \sigma_1 \rho_1^2 - D \sigma \rho_1 \sum_{n=2}^{n_{\max}-1} P_n^* \rho_n. \quad (13)$$

E. Generalized cooperative diffusion

In order to generalize Eq. (9) to any critical size value $i^* > 1$, a second index m should be introduced:

$$\begin{aligned} \frac{\partial O}{\partial t} = & \gamma F \frac{(1-O)}{(1-\rho_{\max})} - \sigma \sum_{n=1}^{i^*} \rho_n \sum_{m=1}^{n_{\max}-1} D_{nm} P_{nm}^* \rho_m \\ & + (1-O) \sum_{n=2}^{i^*} D_{n0} P_{n0}^* \rho_n. \end{aligned} \quad (14)$$

The nm index considers the diffusion of an adatom from a subcritical n -size cluster to m -size cluster, so that the $n0$ index refers to the dissociation of a subcritical n -size cluster always larger than a monomer.

Figure 4(c) shows the occupation dependence on the coverage for every diffusion mechanism described above and the comparison with the random incidence. It is observed that how the aggregation capacity is meaningfully increased as

the diffusion coefficient and directional capture probability are spread out in the corresponding size-differentiated contributions. The figure inset displays how the dimer dissociation enhances the aggregation in a narrow coverage range (0.05–0.15 ML) in which the dimer density becomes important.

The $\rho_1/(O-\rho_1)$ ratio evolutions for the different diffusion mechanisms are showed in Fig. 5(c). As the system aggregation capacity is improved, the monomer to cluster density ratio deviates from the random incidence behavior and gets closer to the dependence previously observed in Fig. 5(b), that was characterized by three regimes. This evolution is due to the appearance and enlargement of a second regime driven by an aggregation-enhanced bounce-back effect, which is able to counterbalance totally or partially the aggregation mechanism. Then, a self-sustained equilibrium between aggregation and desaggregation by bounce back is established during this regime. Contrary to the transient mobility, the bounce back promoted by the cooperative diffusion compensates totally the aggregation, so that $\rho_1/(O-\rho_1)$ ratio remains constant. The decreasing rate of monomer to cluster density ratio depends on the growth dynamics of the clusters. Thus, while the growth rate of a cluster coarsening from transient mobility does not depend on its size; the growth rate of a cluster growing from cooperative diffusion in a nondepleted surrounding area increases exponentially with the cluster size. Consequently, the cluster size distributions produced by these two aggregation mechanisms are different, as well as the magnitudes of their respective bounce-back processes.

V. EXPERIMENTAL DATA FITTING

Once defined and characterized the aggregation mechanisms, it proceeds to fit the previously reported experimental data about metal adsorption on Si(111)7×7 surface [Ag,^{17,21,22} Pb,¹⁹ and Y (Ref. 18)] by using a kinetic Monte Carlo algorithm implemented to collect the different mechanisms. The experimental data fitted in each case, which provide the adjustment physical-meaning parameters, correspond to occupation, preference, and cluster size distribution vs coverage for Ag and Y adsorption, and cluster size distribution at a coverage of $\theta = 0.01$ ML for the Pb case. A single aggregation mechanism, the cooperative diffusion, with a set of parameters varying within a narrow value range (see Table I) was found to be enough to get the best fits of the experimental data corresponding to the three systems. The coverage-dependent occupations fitted for Y and Ag, and reproduced from the fitting parameters for Pb are plotted in Fig. 6.

On the other hand, the nonlocal interactions included in the cooperative diffusion model explain the set of experimental evidences summarized in the Introduction of this work. It should be noted that in spite of these evidences in the case of Ag adsorption, the authors¹⁷ have discarded the cooperative diffusion influence (termed by them as biased thermal diffusion) and have assumed the transient mobility as the operating mechanism on the basis of the nondetection of jumps of a single adatom to its neighboring clusters after

TABLE I. Set of parameters proposed by the groups provider of the experimental data of Y (Ref. 18), Pb (Ref. 19), and Ag (Refs. 17,21 and 22) adsorptions (left field of each column) and those used to fit the data to the cooperative diffusion model (right field). For Y adsorption both sets coincide.

	Y		Pb		Ag	
$\nu_0(\text{s}^{-1})^a$	5×10^9	10^6	5×10^9	5×10^9	5×10^9	5×10^9
i^*	1		1	5	1	
E_d^u (eV)	0.92	0.64	0.84	0.75	0.75	
E_d^f (eV)	0.96	0.64	0.84	0.75 ^c	0.79	
E_b (eV)	0.10		0.07	0.05	0.12	
n_{\max}	5			18	14	
R	0	1	0	1	0	
F (ML/s)	0.005		0.001		0.01	
Mechanism ^b	CD	CA	CD	TM+RD	CD	

^aBased on previous works (Refs. 17 and 18), ν_0 was fixed to $5 \times 10^9 \text{ s}^{-1}$ for the three systems.

^bThe mechanism acronyms correspond to CD, cooperative diffusion; CA, capture area (i.e., transient mobility with $R=r$); TM, transient mobility; and RD, random diffusion.

^c $E_d^f \approx E_d^u$ with $E_d^f - E_d^u \leq 0.05 \text{ eV}$ (Ref.17).

15 min of observation. However, a calculation from their own parameters abridged in Table I shows that even for the random diffusion with an average jump rate for monomers at RT of $\nu = 1.19 \times 10^{-3} \text{ sec}^{-1} \approx 1/14 \text{ min}^{-1}$, at least one of each five monomers surrounded by clusters hops to the position of one of its neighboring clusters after 15 min. This points out to the fact that the reported conclusion could be the result of a lack of experimental statistic.

The value of the preexponential factor of metal adatoms hopping on the Si(111)7×7 surface used to fit the cooperative diffusion model to the experimental data is orders of magnitude lower than those deduced by the transition-state theory ($\sim 10^{13} \text{ s}^{-1}$) Refs. 8 and 9 for the adatom diffusion on metal surfaces. Whereas each lattice site of the model

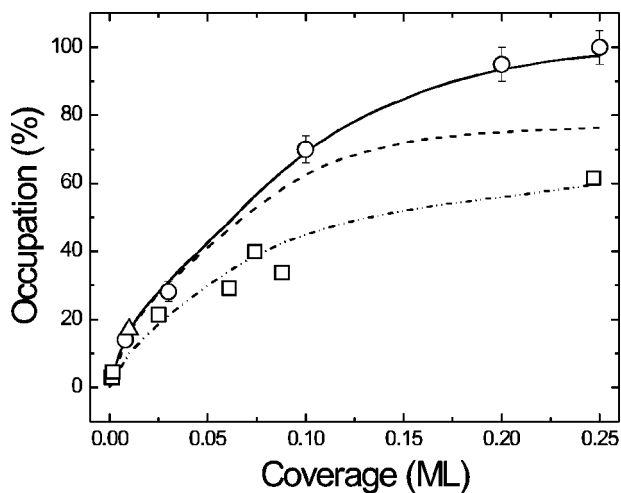


FIG. 6. Coverage dependence of occupation for the three fitted experimental systems [\circ , Y;¹⁸ \triangle , Pb;¹⁹ and \square , Ag (Refs. 21 and 22)] calculated from parameters in Table I.

corresponds to a lateral length of 26.8 Å, a reinterpretation of the physical meaning of the attempt frequency on this model is needed. Based on our model, a feasible explanation for the experimental value as low as 10^6 s^{-1} , reported¹⁹ for the Pb adatoms, is proposed. Anomalies available from the dynamic STM studies have been ascribed to the tip influence²⁶ on the dynamics of the diffusing adatoms. In this case,¹⁹ the tip influence on the dynamics of Pb adatoms adsorbed on the Si(111)7×7 surface was minimized during the experimental procedure of counting the number of jumps per atom and per unit time, and thus, the origin of this disagreement should be looked for elsewhere. Taking into account that monomers are the unique mobile species in this system, characterized by the irreversible aggregation ($i^*=1$), the authors assume the occurrence of only one type of jump (with a unique activation energy proportional to the Arrhenius slope) corresponding to the monomer random diffusion. However, by introducing the cooperative diffusion concept in this system, the monomer diffusion coefficient D is spread out in several D_n coefficients ($n=0, \dots, n_{\max}-1$) as a function of the size of neighboring clusters. Then, the total number of jumps per unit time [$\propto \nu_0 \rho_1 \sum_{n=0}^{n_{\max}-1} \rho_n \exp(-\chi_n/k_B T)$, where $\rho_0 \equiv 1 - O$] ceases satisfying Arrhenius's linear condition. This procedure could induce an underestimation of the diffusion energy barrier and an erroneous preexponential factor.

VI. DISCUSSION

In many of these systems, the random-walk diffusion has proved insufficient to fit the aggregation rates and cluster size distributions.¹⁸ This fact is due to—as it has been pointed out by most of the related publications—the high corrugation ($E_d=0.7-1.0 \text{ eV}$, Ref. 16) presented by the reconstructed Si surface compared with those of metal surfaces²⁷ [e.g., $E_d=0.26 \text{ eV}$ for Pt adatoms on Pt(111), $E_d=0.35 \text{ eV}$ for Cu on Ni(001) or $E_d=0.17 \text{ eV}$ for Ag adatoms on Pt(111)].

On the other hand, it is complicated to justify the presence of transient mobility in the adsorption of thermal metal adatoms (i.e., originated by a nonenergetic technique such as thermal evaporation) on the high corrugate reconstructed Si surface. This drawback is far from being overcome even whether it appeals to the directional nature of the bonds characteristic of the surface reconstruction. In fact, there are neither experimental nor theoretical evidences supporting the transient mobility mechanism of metal adsorbates on semiconductor surfaces. The transient mobility has been shown only in a reduced number of systems such as the adsorption of noble gases²⁸ and oxygen²⁹ on metal surfaces. But in any case, experimental studies have shown the transient mobility as a short-reaching effect, for instance, the average O transient mobility is around two lattice constants on Al(111) (Ref. 29) and Pt(111),³⁰ while the separation between the dissociated Cl-Cl pair on Ni(110) is one lattice constant.³¹ It should be kept in mind, that on the 7×7 reconstructed Si(111) surface, every intercell jump corresponds to a hopping length of 26.8 Å.

Finally, it should be stressed that diffusion mechanisms that depend on the final state as the cooperative contribution have been proposed by several groups to explain their re-

sults. As an example, an activation energy for the random-walk diffusion modified to include the influence of the step-edge barriers to first neighbors have been used since mid 1990s to simulate the development of pyramidal-like mounds on vicinal semiconductor surfaces.³² In spite of this, the physical origin of the cooperative diffusion on semiconductor surfaces remains uncertain, since the nonlocal nature of interactions that induce it and the absence of metal-like delocalized states close to the Fermi level on the Si(111)7×7 surface rule out elastic and electronic contributions to be responsible of this mechanism. Additionally, the possible substrate mediations to these interactions are far from being clarified. Only the following generic features could be picked out so far from the fitting of the experimental data.

(i) The diffusion is modulated by the aggregation centers via nonlocal attractive interactions, which have likely electrostatic nature contributions of the van der Waals type. These interactions would prevail over the dipolar repulsive ones due to the null charge transference between Si and the mobile adsorbates,¹⁸ which would not induce a dipolar momentum in these last ones.

(ii) These interactions modify asymmetrically the activation energy corresponding to the diffusion process as a function of energies of initial and final states of the motion. Thus, the submaximum-size clusters cooperate and enhance the diffusion of the neighboring mobile species originating a

noncompensate particle flux (current) to the aggregation centers.

In conclusion, the cooperative diffusion model constitutes a fair approach to an unified explanation of the adsorption of metal atoms on the Si(111)7×7 surface. Such an explanation, as well as the models focused on the nucleation inside the reconstruction half cells,³³ constitute key pieces in the study of the diffusion and nucleation processes on the reconstructed semiconductor surfaces.

VII. CONCLUSION

The aggregation/desaggregation potential of the mechanisms that control the absorption of metal atoms on the Si(111)7×7 surface was investigated. With this aim, the rate equations describing the evolutions of the surface occupation and the monomer density have been developed for each mechanism. Their numerical solutions were compared with the results obtained by kinetic Monte Carlo simulations. Among several aggregation mechanisms, a cooperative diffusion mechanism, accounting for a reduction of the hopping energy barriers around the aggregation centers due to nonlocal attractive interactions between neighboring adsorbates, was used in order to explain the existing data related to the adsorption of metals on the Si(111)7×7 surface. This fact demonstrates the crucial role played by nonlocal interactions between adsorbates in the interpretation of such results.

*Present address: Institut für Festkörperforschung, Forschungszentrum Jülich, D-52425 Jülich, Germany. Email address: e.vasco.matiias@fz-juelich.de

¹J.A. Venables, *Philos. Mag.* **27**, 697 (1973); J.A. Venables, G.D. Spiller, and M. Hanbücken, *Rep. Prog. Phys.* **47**, 399 (1984); J.A. Venables, *Phys. Rev. B* **36**, 4153 (1987).

²J.V. Barth, H. Brune, B. Fischer, J. Weckesser, and K. Kern, *Phys. Rev. Lett.* **84**, 1732 (2000).

³B. Fischer, H. Brune, J.V. Barth, A. Fricke, and K. Kern, *Phys. Rev. Lett.* **82**, 1732 (1999).

⁴H. Brune, K. Bromann, H. Röder, K. Kern, J. Jacobsen, P. Stoltze, K.J. Jacobsen, and J. Norskov, *Phys. Rev. B* **52**, 14 380 (1995).

⁵J.-R. Chen and R. Gomer, *Surf. Sci.* **94**, 456 (1980); E. Nabighian and X.D. Zhu, *Chem. Phys. Lett.* **316**, 177 (2000).

⁶B.G. Briner, M. Doering, H.-P. Rust, and M. Bradshaw, *Science* (Washington, DC, U.S.) **278**, 257 (1997).

⁷H.A. Kramers, *Physica* (Utrecht) **VII**, 284 (1940); S. Glasstone, K.J. Laidler, and H. Eyring, *The Theory of Rate Processes* (McGraw-Hill, New York, 1941).

⁸U. Kürpick, A. Kara, and T.S. Rahman, *Phys. Rev. Lett.* **78**, 1086 (1997); U. Kürpick and T.S. Rahman, *Phys. Rev. B* **57**, 2482 (1998).

⁹G.H. Vineyard, *J. Phys. Chem. Solids* **3**, 121 (1957); A.F. Voter, *Phys. Rev. B* **34**, 6819 (1986); G. Boisvert and L.J. Lewis, *ibid.* **54**, 2880 (1996).

¹⁰T. Michely, W. Langenkamp, H. Hansen, and C. Busse, *Phys. Rev. Lett.* **86**, 2695 (2001).

¹¹K.A. Fichthorn and M. Scheffler, *Phys. Rev. Lett.* **84**, 5371 (2000).

¹²A. Bogicevic, S. Ovesson, P. Hyldgaard, B.I. Lundqvist, H. Brune, and D.R. Jennison, *Phys. Rev. Lett.* **85**, 1910 (2000); S.

Ovesson, A. Bogicevic, G. Wahnström, and B.I. Lundqvist, *Phys. Rev. B* **64**, 125423 (2001).

¹³J. Repp, F. Moresco, G. Meyer, K.H. Rieder, P. Hyldgaard, and M. Persson, *Phys. Rev. Lett.* **85**, 2981 (2000).

¹⁴N. Knorr, H. Brune, M. Epple, A. Hirstein, M.A. Schneider, and K. Kern, *Phys. Rev. B* **65**, 115420 (2002).

¹⁵C. Polop, H. Hansen, C. Busse, and T. Michely, *Phys. Rev. B* **67**, 193405 (2003).

¹⁶J. Dabrowski and H.-J. Müssig, *Silicon Surfaces and Formation of Interfaces* (World Scientific, Singapore, 2000).

¹⁷J. Myslivecek, P. Sobotík, I. Ot'ádal, T. Jarolímek, and P. Šmilauer, *Phys. Rev. B* **63**, 045403 (2001).

¹⁸C. Polop, E. Vasco, J.A. Martín-Gago, and J.L. Sacedón, *Phys. Rev. B* **66**, 085324 (2002).

¹⁹J.M. Gómez-Rodríguez, J.J. Sáenz, A.M. Baró, J.Y. Veuillen, and R.C. Cinti, *Phys. Rev. Lett.* **76**, 799 (1996).

²⁰O. Custance, I. Brihuega, J.M. Gómez-Rodríguez, and A.M. Baró, *Surf. Sci.* **482-485**, 1406 (2001).

²¹P. Sovotík, I. Ot'ádal, J. Myslivecek, and T. Jarolímek, *Surf. Sci.* **454-456**, 847 (2000).

²²J. Jarolímek, J. Myslivecek, P. Sovotík, and I. Ot'ádal, *Surf. Sci.* **482-485**, 386 (2001).

²³U.K. Köhler, J.E. Demuth, and R.J. Hamers, *Phys. Rev. Lett.* **60**, 2499 (1988); St. Tosch and H. Neddermeyer, *ibid.* **61**, 349 (1988).

²⁴J.T. Kindt, J.C. Tully, M. Head-Gordon, and M.A. Gomez, *J. Chem. Phys.* **109**, 3629 (1998).

²⁵C.C. Chang, X.D. Wu, A. Inam, D.M. Hwang, T. Venkatesan, P. Barboux, and J.M. Tarascon, *Appl. Phys. Lett.* **53**, 517 (1988); B. Dam and B. Stäuble-Pümpin, *J. Mater. Sci.* **9**, 217 (1998).

²⁶L.J. Whitman, J.A. Stroschio, R.A. Dragoset, and R.J. Celotta, *Sci-*

- ence (Washington, DC, U.S.) **251**, 1206 (1991); Y.W. Mo, Phys. Rev. Lett. **71**, 2923 (1993).
- ²⁷M. Bott, M. Hohage, M. Morgenstern, Th. Michely, and G. Comsa, Phys. Rev. Lett. **76**, 1304 (1996); B. Müller, L. Nedelmann, B. Fischer, H. Brune, and K. Kern, Phys. Rev. B **54**, 17 858 (1996); H. Brune, G.S. Bales, J. Jacobsen, C. Boragno, and K. Kern, *ibid.* **60**, 5991 (1999).
- ²⁸P.S. Weiss and D.M. Eigler, Phys. Rev. Lett. **69**, 2240 (1992); P. Zeppenfeld, J. George, M. Bchel, R. David, and G. Comsa, Surf. Sci. **318**, L1187 (1994).
- ²⁹M. Schmid, G. Leonardelli, R. Tschelie Bnig, A. Biedermann, and P. Varga, Surf. Sci. **478**, L355 (2001).
- ³⁰J. Wintterlin, R. Schuster, and G. Ertl, Phys. Rev. Lett. **77**, 123 (1996).
- ³¹T.W. Fishlock, J.B. Pethica, F.H. Jones, R.G. Egdell, and J.S. Foord, Surf. Sci. **377-379**, 629 (1997).
- ³²P. Smilauer and D.D. Vvedensky, Phys. Rev. B **52**, 14 263 (1995).
- ³³K. Cho and E. Kaxiras, Europhys. Lett. **39**, 287 (1997); O. Custance, S. Brochard, I. Brihuega, E. Artacho, J.M. Soler, J.M. Gómez-Rodríguez, and A.M. Baró (unpublished).